Nuclear shell model and analytical SU(3) description of ^{28}Si

Author: Dorian Grzegorz Frycz
Facultat de Física, Universitat de Barcelona, Diagonal 645, 08028 Barcelona, Spain.

Advisor: Javier Menéndez Sánchez

Abstract: We analyze the ^{28}Si nucleus using an analytical SU(3)-based model as well as state of the art numerical shell model calculations. In principle, spherical, oblate and prolate structures can coexist at low energies. However, we found that the spherical shape in ^{28}Si does not survive because the $1d_{5/2}$-$2s_{1/2}$ nearly degenerated doublet gains huge amounts of quadrupole correlations, which favors deformed bands. Although the standard USDB interaction reproduces the oblate ground state and the vibrational band, it fails at establishing a prolate band. A modification of the USDB interaction must be introduced to reproduce the experimental spectrum. Our calculations suggest that the oblate ground state is mostly 0p-0h, whereas the prolate band consists mainly of 4p-4h excitations into the $1d_{3/2}$ orbital.

I. INTRODUCTION

Atomic nuclei are self-bound systems comprised of strongly interacting nucleons. Although the premise might be simple-looking, it gives rise to spectacular complex phenomena, which can be inferred from experimental data. Amidst others, the coexistence of spherical states, normal deformed (ND) and superdeformed (SD) rotational bands at low energy states has been a puzzling topic of interest. These names refer to the intrinsic shape in the laboratory frame of the states of the band. These rotational bands are due to collective behavior rather than single-particle excitations, which points out to the importance of collectivity in nuclei.

Hitherto, medium-mass nuclei such as ^{40}Ca [1], ^{40}Ar [2] [3], ^{42}Ca [4] and ^{36}Ar [5] have been found to exhibit competition among spherical and unlike kinds of deformed states. In this work, we focus on ^{28}Si, which is an even-even nucleus formed by 14 protons and 14 neutrons. Several studies [6–8] show that the 3 lowest-lying 0^+ states are bandheads of an oblate rotational band, a vibrational band and a prolate rotational band, respectively. Prolate shapes are axially symmetric spheroids elongated along one axis while oblate ones are flattened. Therefore, ^{28}Si presents shape coexistence between prolate and oblate states, whereas the spherical one does not survive. The observed spectrum is represented on Fig. 1 (left panel).

In this work, our aim is to understand experimental data both from a simple analytical SU(3) scheme (section II) and state of the art shell model computational calculations (section III).

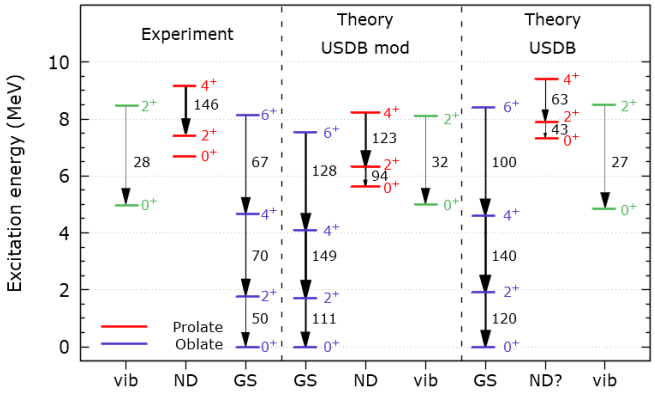

FIG. 1: Band structure of the lowest-lying positive parity states of ^{28}Si: left, experiment [6]; center, calculation using the USDB_mod interaction and right, using USDB. The arrows indicate in-band $B(E2)$ transition strenghts (e^2 fm^4), with larger values associated to more deformed shapes. The labels "vib", "ND" and "GS" stand for vibrational band, normal deformed band and ground state, respectively.

II. ANALYTICAL SU(3) MODEL

A. Deformation in nuclei

Rotational bands are characteristic of non-spherical nuclei, which acquire a permanent deformed shape due to their rotation in the intrinsic frame of reference [9]. This resembles an ideal rotor with a constant moment of inertia I. The kinetic energy (E_{kin}) depends on the value of $\vec{L}^2$, where $\vec{L}$ is the orbital angular momentum of the rotor. Thus, taking the usual quantum approach, one ends up with $E_{kin} = \frac{L(L+1)}{2I}$, where L is the orbital quantum number (we consider $\hbar = 1$). Extending this analysis to the coupled scheme $\vec{J} = \vec{L} + \vec{S}$, where $\vec{J}$ is the total angular momentum and $\vec{S}$ is the spin, excited states in the laboratory frame follow a sequence proportional to $J(J+1)$, where J is the total angular momentum quantum number.

The electric quadrupole moment denotes the deformation of the nucleus. For spherical shapes, the quadrupole moment vanishes. In the laboratory frame, it is defined by [10]

$$Q_{spec} \equiv \sqrt{\frac{16\pi}{5}} \sqrt{\frac{J(2J-1)}{(J+1)(2J+1)(2J+3)}} (J||Q_{20}||J), \quad (1)$$

where $Q_{20} = \sum_{j=1}^{A} e_j r_j^2 Y_{20}(\theta_j, \phi_j)$: e_j are the effective

nuclear charges, A is the mass number, Y_{20} is the spherical harmonic and (r_j, θ_j, ϕ_j) are the spherical coordinates of the j^{th} nucleon. The notation $(J||Q_{20}||J)$ indicates a reduced matrix element [10]. Additionally, the states that belong to a rotational band are connected by strong electromagnetic transitions, quantified by the reduced $B(E2)$ transition strength between an initial (J_i) and a final (J_f) state:

$$B(E2; J_i \to J_f) \equiv \frac{1}{2J_i + 1} |(J_i||Q_{20}||J_f)|^2. \tag{2}$$

It is possible to measure both $B(E2)$ transitions as well as the Q_{spec}'s, which allows us to compute the values of the intrinsic quadrupole moments [1]:

$$Q_{0,t} = \pm \sqrt{\frac{16\pi B(E2, J \to J-2)}{5|\langle J020|J-2,0\rangle|^2}}, \tag{3}$$

$$Q_{0,s} = \frac{-(2J+3)}{J} Q_{spec}, \tag{4}$$

where $\langle J020|J-2,0\rangle$ is a Clebsch-Gordan coefficient. Positive intrinsic quadrupole moments are associated to prolate shapes while negative ones are oblate. States of a rotational band with well-established intrinsic quadrupole moment fulfill $Q_{0,s} \approx Q_{0,t}$.

Finally, it is useful to define a deformation parameter β that allows one to compare different nuclei:

$$\beta = \sqrt{\frac{\pi}{5}} \frac{Q}{R^2 Ze}; \quad R = 1.2A^{1/3}\text{fm}, \tag{5}$$

where Z is the atomic number and e is the elementary charge. Throughout the study we consider that a state is normal deformed if $0.3 \lesssim \beta \lesssim 0.4$ and superdeformed if $\beta \gtrsim 0.6$.

B. Spherical mean field

Through the years, plenty of methods have been proposed to explain the structure and dynamics of nuclei. Notably, one of the most common knowledge might be the spherical mean field. In this approach, the two-body nucleon interaction is approximated by a mean field harmonic oscillator potential [11]. This choice stems from the multiple symmetries that it possesses. Nevertheless, orbital $\vec{l} \cdot \vec{l}$ and spin-orbit (SO) $\vec{l} \cdot \vec{s}$ terms must be included to accommodate experimental evidence, such as magic numbers. Thus, the potential energy representing the nuclear mean field ends up being

$$U(r) = \frac{1}{2}\omega r^2 + A\vec{l} \cdot \vec{l} + B\vec{l} \cdot \vec{s}, \tag{6}$$

where ω is the angular frequency, $\vec{l}$ is the orbital angular momentum, $\vec{s}$ is the spin and A and B are constants. The resulting single-particle levels are represented in Fig. 2. Hence, for this "independent particle model" the ^{28}Si

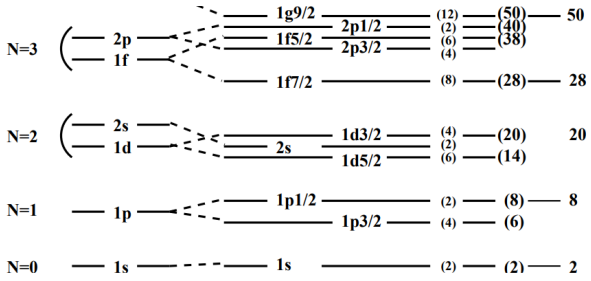

FIG. 2: Spherical mean field single-particle orbitals for both protons and neutrons. From left to right: major harmonic oscillator shells and spin-orbit splitting. Taken from [12].

ground state (GS) is obtained by independently filling the 14 protons and 14 neutrons up to the $1d_{5/2}$ orbit (included). This would lead to a spherical state, which does not agree with the experimental spectrum of ^{28}Si (see Fig. 1). Moreover, most nuclei are deformed and a new formalism must be used to explain this phenomenon. Elliott's SU(3) model draws on the symmetries of the harmonic oscillator to explain this behavior.

C. SU(3) model

Deformation in nuclei can be incorporated by introducing quadrupolar interactions $-2q^{20} \cdot 2q^{20}$ to the nuclear Hamiltonian, where $q^{20} \equiv r^2\sqrt{4\pi/5}\ Y^{20}$. Elliott's SU(3) scheme [13] considers a strong presence of quadrupole interactions restricted to a major harmonic oscillator shell with quantum number N. Then, configuration mixing, in this restricted space, is taken into account to maximize the intrinsic quadrupolar moment $Q_0 = 2q^{20} = (2n_z - n_x - n_y)b^2$, where n_i are the cartesian components, $n_x + n_y + n_z = N$, and the harmonic oscillator parameter $b^2 \approx 41.4/(45A^{-1/3} - 25A^{-2/3})$ fm^2 is fitted to measured nuclear charge radii [10]; for ^{28}Si $b^2 \approx 3.42$ fm^2. The states of a rotational band share this intrinsic deformed shape. For instance, in the sd shell (N=2), we end up with the quadrupole SU(3) diagram of Fig. 3, a) panel. The orbits that appear have fourfold degeneracy, due to spin and isospin projections.

Let us apply the SU(3) scheme to ^{28}Si. In the independent particle model, a spherical state with 12 nucleons occupies the lowest-lying $1d_{5/2}$ orbit. For a single orbit, with total angular momentum number j and projection m, Q_0 is given by [14]

$$Q_0 = \sum_m (N + 3/2) \frac{j(j+1) - 3m^2}{2j(j+1)} b^2. \tag{7}$$

Indeed, if we add up all the contributions of a closed shell, then $Q_0 = 0$. On the other hand, Elliott's scheme allows the 12 particles to distribute among the sd shell orbits, such that $|Q_0|$ is maximal. The quadrupole correlation energy scales as the square of the intrinsic electric quadrupole moment Q_0. Thus, configurations that

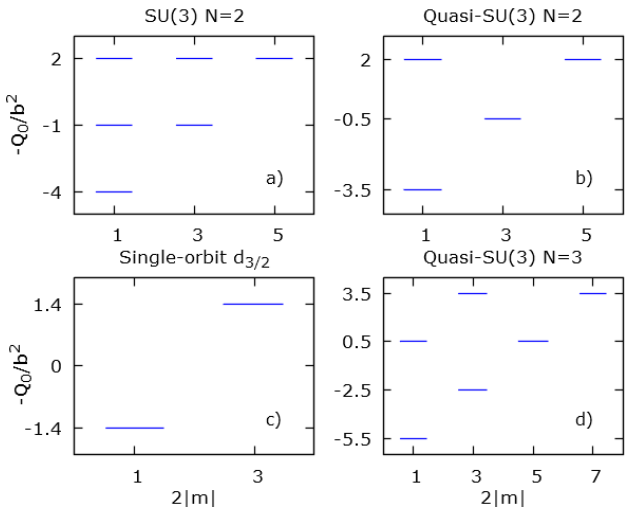

FIG. 3: Quadrupole diagrams of the different SU(3) variants considered in this work. The (-) quadrupole moment Q_0 is represented for each available $2|m|$ value, where m is the projection of the total angular number j. Prolate states are obtained by filling from below and oblate ones from above.

maximize Q_0 may have the chance to overcome the corresponding single-particle energy differences. The prolate state is built by filling diagram 3 a) from below resulting in $Q_0 = (4\cdot4+1\cdot8+3)b^2 = 27b^2$, where a $3b^2$ term must be added by comparison with ideal rotors [15]. Likewise, the oblate state also has $Q_0 = (-2\cdot12-3)b^2 = -27b^2$. We recover dimensions multiplying Q_0 by the nuclear effective charges: $e_\pi = 1.5e$ for protons and $e_\nu = 0.5e$ for neutrons. Then, $|Q_0| = (12\cdot1.5e + 12\cdot0.5e + 3e)\cdot3.42$ fm^2=92.3 e fm^2. Therefore, the SU(3) model predicts ^{28}Si with degenerate oblate/prolate states with the above values. Nevertheless, as shown in Fig. 1, the experimental oblate ground state and the ND prolate band are almost 7 MeV apart.

D. SU(3) variants

Thus far, Elliott's pure SU(3) approach does consider all the major harmonic oscillator orbits degenerate, albeit SO splitting can be quite significant. Therefore, SU(3) overestimates quadrupole correlations. However, other SU(3) schemes [14] exist that deal with this issue, reducing the symmetry in exchange of a more realistic view.

One of the SU(3) variants is the quasi-SU(3) scheme, tailored for $\Delta j = 2$ orbitals. This scheme exploits that $\Delta j = 1$ single-particle matrix elements of q^{20} are weaker than $\Delta j = 2$ ones [16]. For instance, in the sd shell this scheme involves the $1d_{5/2}$-$2s_{1/2}$ doublet, as represented in Fig. 3 b).

If an orbit is quite far apart from the others, the single-orbit may be the best fit. In this case, the quadruple moment is shown in Fig. 3 c), following Eq. (7).

A $(d_{5/2}$-$s_{1/2})$+$d_{3/2}$ prescription is best suited for ^{28}Si since $d_{5/2}$-$s_{1/2}$ are only 0.7 MeV apart in comparison to $\sim$5 MeV between the doublet and $d_{3/2}$ (single-particle energies extracted from the USDB interaction [17]). The np-nh notation stands for promoting n particles, protons or neutrons, from the $d_{5/2}$-$s_{1/2}$ orbitals to the $d_{3/2}$ one. The corresponding quadrupole moments are collected in table I. For example, to obtain the oblate 0p-0h configuration we fill diagram 3 b) with 12 particles from above $Q_0 = (8\cdot(-2)+4\cdot0.5-3)/2\cdot(0.5+1.5)e\cdot(3.42)$ fm^2= -58.1 e fm^2 or for the prolate 4p-4h configuration $Q_0 = (4\cdot3.5+4\cdot0.5+4\cdot1.4+3)/2\cdot(0.5+1.5)e\cdot(3.42)$ fm^2= 84.1 e fm^2. The large Q_0 for the oblate 0p-0h configuration is remarkable, because just by adding the $s_{1/2}$ orbit there is a huge gain of correlation with respect to the filled $d_{5/2}$ spherical picture. Since the $s_{1/2}$ orbit is very close to the $d_{5/2}$ and the gain in collectivity is large, the system gravitates towards an oblate deformed shape instead of the spherical one. Moreover, the experimental data is quite close to our prediction: $Q_{0,t} = -57.3$ e fm^2 (β =0.25) [7], although this does not imply that the real GS is that simple.

Table I indicates that with respect to ND bands ($0.3 \lesssim \beta \lesssim 0.4$), the best candidates are the oblate 2p-2h and 4p-4h configurations. In the former, 13 e fm^2 are gained with respect to the 0p-0h configuration. In the latter, the difference is also 13 e fm^2 with respect to 2p-2h. However, as the correlation energy scales quadratically with the quadrupole moment and the np-nh single-particle energy is linear with the amount of excited particles, the 4p-4h might be a better candidate, provided that the quadrupole force is strong enough. The remaining 6p-6h and 8p-8h configurations are disfavored due to higher single-particle energy and smaller $|Q_0|$.

III. NUCLEAR SHELL MODEL

The starting point of the nuclear shell model is the spherical mean field, which sets the single-particle basis. However, the full space is intractable due to the very

TABLE I: Quadrupole moments (e fm^2) for the experimental GS and ND bands, the possible spherical state and the np-nh configurations in the analytical $(d_{5/2}$-$s_{1/2})$+$d_{3/2}$ scheme and the shell model numerical calculations. We also present SU(3) predicted values as well as numerical GS and the possible ND results obtained with the USDB interaction.

$Q_{0,\text{spherical}}$		$Q_{\text{exp,GS}}$			$Q_{\text{exp,ND}}$	
0		**-57.3±0.7**			**70±7**	
Analytical	0p-0h	2p-2h	4p-4h	6p-6h	8p-8h	Pure SU(3)
$Q_{0,\text{prolate}}$	37.6	60.9	**84.1**	71.1	58.1	**92.3**
$Q_{0,\text{oblate}}$	**-58.1**	-71.1	**-84.1**	-60.9	-37.6	**-92.3**
Numerical	0p-0h	2p-2h	4p-4h	6p-6h	8p-8h	GS	ND?
$Q_{0t,\text{USDB}}$	**±41.6**	±49.4	**±68.2**	±53.9	±45.2	**±70.7**	**±46.6**
$Q_{0s,\text{USDB}}$	**-45.7**	16.0	**66.4**	±46.4	9.8	**-73.0**	**31.2**

large number of Slater determinants, because shell model wave functions are linear combinations of Slater determinants. The solution is to restrict the many-body problem to a valence space, close to the Fermi level of the independent particle model. As a result, we end up with an inert core, with levels that are forced to remain always full, and an empty external space. The valence space is in between and contains the remaining nucleons. Now, an effective interaction (H_{eff}) tailored for the valence space is needed. This is the residual interaction between nucleons.

For ^{28}Si, a natural valence space is the sd-shell. Hence, we have an ^{16}O inert core and 12 particles to distribute among the $d_{5/2}$, $s_{1/2}$ and $d_{3/2}$ orbits. The interaction of choice is the universal sd-shell interaction (USDB) [17], which is adapted to medium-mass nuclei in this region. In general, USDB describes very successfully the level structure of nuclei in the sd-shell. Finally, we use the ANTOINE shell model code [11, 18] to solve the Schrödinger equation to obtain the eigenvalues and eigenstates in the valence space:

$$H_{eff}|J\rangle = E_J|J\rangle. \tag{8}$$

ANTOINE builds up all the necessary Slater determinants in the valence space and diagonalizes the Hamiltonian via a tridiagonal Lanczos method [12].

A. Fixed np-nh calculations

Calculations of np-nh configurations are restricted to a truncated space where n particles are promoted to a space with higher single-particle energies. ANTOINE provides the electric $B(E2)$ transition strengths between different J levels, as well as the values of Q_{spec}. The Q_0 values (table I) are extracted from these two methods and they should agree if the deformation of the band is well established.

Table I gives values of Q_{0t} and Q_{0s} close to each other except for 2p-2h and 8p-8h, which means that there is no intrinsic deformed state associated to these configurations. The 0p-0h configuration is oblate, same as the experimental GS and the analytical prediction. Now, for the 4p-4h USDB predicts a prolate band, albeit the analytical model considers prolate and oblate deformations degenerate. This breaking in degeneracy might be due to nuclear interaction effects that are beyond the single-particle energies and the quadrupole interactions considered in the analytical scheme.

B. Full sd space calculations

The np-nh configurations mix in the unrestricted sd space to minimize the state energy. This effect is incredibly important in nuclei. For instance, the 0p-0h state lies 7.5 MeV above the ground state when configuration mixing is allowed.

With the USDB interaction we find a well-established oblate rotational band, on top of the ground state: the energies follow a $J(J+1)$ sequence, the $B(E2)$'s fulfill Eq. (3) and the Q_{spec}'s follow Eq. (4). The quadrupole moments are $|Q_{0t}(2^+_{GS} \rightarrow 0^+_{GS})| = 70.7\ e\ \text{fm}^2$ and $Q_{0s}(2^+_{GS}) = -73.0\ e\ \text{fm}^2$. However, they overestimate the experimental value $Q_{0,exp} = -57.3 \pm 0.3\ e\ \text{fm}^2$ [7].

Another interesting property is the average occupation number of each orbit. For the 0^+_{GS} we find that, on average, there are 9.32 particles in $d_{5/2}$, 1.25 in $s_{1/2}$ and 1.43 in $d_{3/2}$. In contrast, for a spherical state we would expect all 12 particles to be in $d_{5/2}$ and for the 0p-0h the $d_{3/2}$ should be empty. Indeed, the situation is quite complex and our analytical schemes are just an approximation.

Experimental data shows that there is a ND prolate band. Nonetheless, the band is not predicted by the USDB interaction. There might be some states that resemble a band but the in-band transition strengths are way too weak, as shown in Fig. 1. This means that the 4p-4h configuration in table I is diluted in the sd-shell space. In Fig. 4 (top panel) we can observe that the 7.3 MeV, 0^+_3 state only has 10% of the 4p-4h configuration. This component is not enough to produce a solid rotational band that could be identified with the experimental one.

C. Modification of the nuclear interaction

The USDB interaction fails at establishing a ND prolate band. To improve this deficiency we modify the gap energy between the $d_{5/2}$-$s_{1/2}$ and $d_{3/2}$ single-particle energies. We expect that this change will allow the correlation energy to overcome the single-particle one sufficiently to establish a rotational band. This change will not affect the quadrupole moment of the np-nh configu-

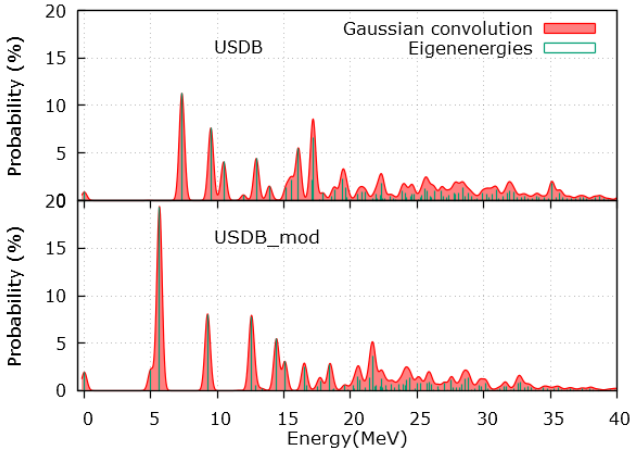

FIG. 4: Probability of the 4p-4h configuration (%) in the full sd-shell states, with each eigenstate convoluted with Gaussians of 200 keV width: top panel, USDB interaction; bottom panel, USDB_mod.

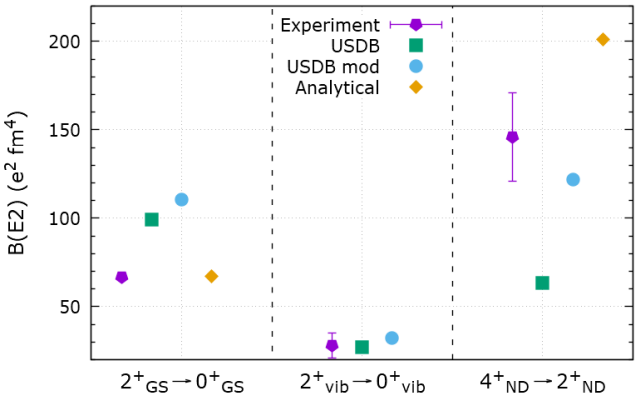

FIG. 5: In-band $B(E2)$ values. Experimental values compared to the USDB, USDB_mod and analytical calculations.

rations from table I. Instead, it allows the structure to survive the configuration mixing in the full sd space.

Our interaction, which we call USDB_mod, is adjusted to $E_{gap} = 4.5$ MeV (for USDB $E_{gap} = 5.9$ MeV) between the $d_{5/2}$-$s_{1/2}$ and $d_{3/2}$ orbits. This choice is not unique but it balances out the $B(E2)$ experimental transitions, the state energies and it keeps the vibrational 0^+_{vib} state below the 0^+_{ND} one. Remarkably, by lowering the gap 1.4 MeV, the presence of 4p-4h in the 0^+_3 state shown in Fig. 4 increases from 10% to 20%. This is sufficient to establish a well-behaved rotational band.

The corresponding spectra are represented in Fig. 1. In Fig. 5 we collect all the $B(E2)$ values obtained thus far. The ND band shown at the right of the figure is described correctly by the USDB_mod interaction while USDB fails at creating this band and the analytical value $B(E2, 4^+_{ND} \rightarrow 2^+_{ND}) = 201\ e^2\ \text{fm}^4$ overestimates the experimental value. The vibrational band is described well both in USDB and USDB_mod. Finally, the $B(E2, 2^+_{GS} \rightarrow 0^+_{GS})$ is compatible with the analytical model while the numerical calculations are overestimated. Even though USDB_mod has a slightly worse prediction for the GS, this is more than compensated by achieving a solid ND band. Overall, figures 1 and 5 highlight the challenge of describing the coexistence of states with different intrinsic deformation in ^{28}Si.

IV. CONCLUSIONS AND OUTLOOK

In this work, we have focused on the nuclear structure of ^{28}Si. First, we have seen how an analytical SU(3)-based scheme can naturally explain which rotational bands appear on the spectrum. We have shown that the $(d_{5/2}$-$s_{1/2})$+$d_{3/2}$ space predicts an oblate ground state mainly composed of 0p-0h configurations and a normal deformed band based on 4p-4h excitations. Numerical fixed np-nh calculations point out to the same conclusions as the analytical model. However, in the full sd space calculations the USDB interaction for ^{28}Si describes well the ground state and the vibrational band, but the normal deformed band is missing due to configuration mixing. Our solution is to adjust a new interaction so that the gap between the $d_{5/2}$-$s_{1/2}$ and $d_{3/2}$ orbitals is reduced by 1.4 MeV to better accommodate experimental values. With this change, the ND band survives and describes very well the experimental data. Nonetheless, the GS $B(E2)$ transition strengths are slightly overestimated.

For future work, we would like to explore a possible superdeformed band in ^{28}Si, which has been suggested theoretically [8] and recently explored experimentally [6]. We have seen that excitations within the sd shell lead to intrinsic shapes limited to $\beta < 0.4$, so the pf shell is needed. Analytically, a promising prescription is to allow excitations from the $1d_{5/2}$-$2s_{1/2}$ to the $1f_{7/2}$-$2p_{3/2}$ nearly degenerated doublet, which features a prolate 4p-4h configuration with $\beta = 0.76$, obtained following Fig. 3 d). As a final step, we plan to carry out shell model calculations with an interaction suitable to the sd-pf space.

Acknowledgements

First, I would like to express my gratitude to my advisor Javier Menéndez, who shared his knowledge and guided me throughout this research, as well as Arnau Rios for his advice. Finally, I want to thank my friends and family for their overall support, which helped me out a lot.

[1] Caurier, E., et al. Phys Rev C 75 (2007): 054317.
[2] Taniguchi, Y., et al. Phys Rev C 82 (2010): 011302.
[3] Yang, Y., et al. Eur Phys J A 54 (2018): 1-8.
[4] Hadyńska-Klęk, K., et al. Phys Rev Lett 117 (2016): 062501.
[5] Svensson, C. E., et al. Phys Rev Lett 85 (2000): 2693.
[6] Morris, L., et al. Phys Rev C 104 (2021): 054323.
[7] Endt, P. M. Nucl Phys A 633 (1998): 1-220.
[8] Taniguchi, Y., et al. Phys Rev C 80 (2009): 044316.
[9] Krane, K. S. (1991). Introductory nuclear physics. John Wiley & Sons.
[10] Suhonen, J. (2007). From nucleons to nucleus: concepts of microscopic nuclear theory. Springer.
[11] Caurier, E., et al. Rev Mod Phys 77 (2005): 427.
[12] Poves, A., Nowacki, F. Springer, Berlin, Heidelberg, 2001. 70-101.
[13] Elliott, J. P. Proc R Soc Lon Ser-A 245 (1958): 128-145.
[14] Zuker, A. P., et al. Phys Rev C 92 (2015): 024320.
[15] Retamosa, J., et al. Nucl Phys A 511 (1990): 221-250.
[16] Zuker, A. P., et al. Phys Rev C 52 (1995): R1741.
[17] Richter, W. A., et al. Phys Rev C 78 (2008): 064302.
[18] Caurier, E. (1989). Shell model code ANTOINE. IReS, Strasbourg, 2002.